Retrieval of CO Relative Column Abundance in the Martian Thermosphere From FUV Disk Observations by EMM EMUS

J. S. Evans, J. Correira, J. Deighan, S. Jain, H. Al Matroushi, H. Al Mazmi, M. Chaffin, S. Curry, S. England, F. Eparvier, et al.

Geophysical Research Letters®

Retrieval of CO Relative Column Abundance in the Martian Thermosphere From FUV Disk Observations by EMM EMUS

J. S. Evans[1] , **J. Correira[1]** , **J. Deighan[2]** , **S. Jain[2]** , **H. Al Matroushi[3]** , **H. Al Mazmi[4]** , **M. Chaffin[2]** , **S. Curry[5]** , **S. England[6]** , **F. Eparvier[2]** , **M. Fillingim[5]** , **F. Forget[7]** , **G. Holsclaw[2]** , **R. Lillis[5]** , **F. Lootah[3]** , and **E. Thiemann[2]**

[1]Computational Physics, Inc., Springfield, VA, USA, [2]Laboratory for Atmospheric and Space Physics, University of Colorado, Boulder, CO, USA, [3]Mohammed Bin Rashid Space Center, Dubai, UAE, [4]United Arab Emirates Space Agency, Abu Dhabi, UAE, [5]Space Sciences Laboratory, University of California Berkeley, Berkeley, CA, USA, [6]Virginia Tech, Blacksburg, VA, USA, [7]Laboratoire de Météorologie Dynamique, Institut Pierre Simon Laplace Sorbonne Université, Paris, France

Abstract Carbon monoxide (CO) is a sensitive tracer of the thermal profile and winds in Mars' middle atmosphere and the chemistry that balances CO_2 in the whole atmosphere of Mars. The Emirates Ultraviolet Spectrometer (EMUS) onboard the Emirates Mars Mission Hope probe images Mars at ultraviolet wavelengths from approximately 100 to 170 nm. $\Sigma CO/CO_2$, the column density ratio of CO to carbon dioxide, provides a sensitive measure of CO relative variability within the Martian thermosphere. Derived from the heritage of $\Sigma O/N_2$ used at Earth, the $\Sigma CO/CO_2$ algorithm uses emission from the CO Fourth Positive Group band system to derive the relative column abundance of CO above ~70 km. We describe the EMUS $\Sigma CO/CO_2$ algorithm, review the Level 3 data product, and discuss preliminary validation of the algorithm. The $\Sigma CO/CO_2$ algorithm produces column density ratios that characterize the spatial structure and relative variability of CO abundance in the Martian thermosphere.

Plain Language Summary The Emirates Mars Ultraviolet Spectrometer onboard the Emirates Mars Mission observes light in a wavelength region referred to as far ultraviolet. This study focuses on far ultraviolet light that is produced by carbon monoxide (CO). Observations of far ultraviolet light can be used to determine the relative abundance of CO in the upper atmosphere of Mars. Variations in the relative abundance of CO over time and across different locations can provide valuable information regarding the temperatures and winds in the middle atmosphere of Mars, as well as the chemistry that balances the whole atmosphere of Mars. This study presents a method for converting observations of far ultraviolet light into relative abundances of CO in the upper atmosphere of Mars.

1. Introduction

Carbon monoxide (CO) plays a major role in the chemical cycles of CO_2, hydrogen, and oxygen, and is a tracer of the thermal profile and winds in the Martian middle atmosphere. With a mean lifetime of about 6 Mars years (Krasnopolsky, 2007), CO is produced primarily through CO_2 photolysis in the middle atmosphere and is effectively lost in the lower atmosphere through catalysis by the OH radical produced by water vapor (H_2O) photolysis. Given such a long lifetime (relative to one Mars year), no variation of CO with local time is expected. However, as an incondensable, CO is expected to vary both locally and temporally with Mars season. The spatial distribution of CO is therefore an important quantity that can be used to constrain models of photochemical and dynamical processes in the Martian atmosphere. Indeed, the model predicted long-term equilibrium value for the CO volume mixing ratio is smaller than observed by a factor two to four (Lefèvre & Krasnopolsky, 2017). This disagreement suggests that our understanding of Martian atmospheric chemistry remains incomplete (Olsen et al., 2021).

A CO mixing ratio of 800 ± 300 ppmv was detected on Mars by Kaplan et al. (1969) using high-resolution Fourier transform spectra. Krasnopolsky (2003) observed variations of the CO mixing ratio in the lowest scale height at $L_s = 112°$ using lines of the CO (3-0) band at 1.58 μm. Condensation of CO_2 in the southern polar and subpolar regions resulting in enrichment of incondensable gases (N_2, Ar, O_2, CO, H_2, CH_4, etc.) was later confirmed by Sprague et al. (2004, 2012) in observations of Ar using the gamma ray spectrometer on the Mars Odyssey orbiter. Seasonal variation of CO at Hellas Basin was studied by Encrenaz et al. (2006) using the Omega low-resolution imaging spectrograph onboard the Mars Express orbiter. The most extensive coverage of Mars CO

to date was produced with the Compact Reconnaissance Imaging Spectrometer (Smith et al., 2009, 2018; Holmes et al., 2019), which found a mean mixing ratio at mid-latitudes of around 800 ppmv, with seasonal low-latitude enhancements reaching ~1,000 ppmv around $L_s = 180°$.

More recently, the Neutral Gas and Ion Mass Spectrometer (NGIMS; Mahaffy et al., 2015) onboard the Mars Atmosphere and Volatile Evolution (MAVEN; Jakosky et al., 2015) satellite has made in situ measurements of CO abundance between 140 and 350 km during the periapse segment of MAVEN orbits. However, these density measurements are restricted to the upper thermosphere and carry large uncertainties below 160 km (Olsen et al., 2021). Also reported recently are Mars equinox observations of vertical profiles of CO from 10 to 120 km covering a broad range of latitudes from the Atmospheric Chemistry Suite (ACS) onboard the ExoMars Trace Gas Orbiter (TGO; Olsen et al., 2021). These results indicate an equatorial CO mixing ratio of ~1,000 ppmv (10–80 km) that increases to more than 3,000 ppmv toward the polar regions. Direct comparisons between ACS MIR and NGIMS can only be made cautiously, however, because the uncertainty of ACS MIR retrievals is very large above 100 km (Olsen et al., 2021). Clearly there is a significant and important gap in knowledge of the CO abundance from about 100 to 160 km. To complete our understanding of the chemical cycles of CO_2, hydrogen, and oxygen in the Martian atmosphere this gap must be filled.

The Emirates Ultraviolet Spectrometer (EMUS; Holsclaw et al., 2021) onboard the Emirates Mars Mission (EMM; Almatroushi et al., 2021; Amiri et al., 2022) Hope probe images Mars at extreme- and far-ultraviolet wavelengths extending from approximately 100 to 170 nm. The EMUS $\Sigma CO/CO_2$ algorithm (where Σ indicates a slant path integral) provides a measure of relative composition variability within the Martian thermosphere by deriving the column abundance of CO above a fixed CO_2 reference column density of 5×10^{19} cm^{-2} (corresponding to an altitude of ~70 km) from EMUS disk images. The $\Sigma CO/CO_2$ algorithm traces its origins to the $\Sigma O/N_2$ algorithm used at Earth for studying relative variability in atomic oxygen abundance from remote sensing observations (Correira et al., 2021; Evans et al., 1995; Strickland et al., 1995). In a similar manner, relative composition can be inferred for the Martian atmosphere using CO and carbon dioxide.

The $\Sigma CO/CO_2$ algorithm uses a lookup table approach by first generating a series of model atmospheres that span the expected range of physically realistic atmospheres. The AURIC model (Evans et al., 2015; Stevens et al., 2015; Strickland et al., 1999) is then used to calculate column emission rates and spectral radiances as functions of $\Sigma CO/CO_2$ column density ratio, solar zenith angle, and emission angle for the range of input model atmospheres. When used with EMUS observations, the lookup table provides a unique mapping from intensity ratio to $\Sigma CO/CO_2$ column density ratio for a given solar zenith angle and emission angle. Intensities from carefully selected bands of the optically allowed CO Fourth Positive Group (4PG) band system ($A^1\Pi \rightarrow X^1\Sigma^+$) are used as a signature of CO variability (Barth et al., 1969; Feldman et al., 2000; Jain et al., 2015; Leblanc et al., 2006).

In this paper, we describe the EMUS Level 3 science data product $\Sigma CO/CO_2$. Section 2 provides further details on the EMUS instrument and observations relevant to deriving $\Sigma CO/CO_2$ and discusses the FUV dayglow features observed by EMUS. As the algorithm used for generating EMUS Level 3 $\Sigma CO/CO_2$ data products relies upon the well-established work of Strickland et al. (1995), Section 4 briefly reviews the essential points, provides details about specific application to EMUS disk observations, and discusses the lookup table that drives the algorithm. Validation of column density ratios using a global circulation model is discussed in Section 5. Finally, we summarize our key findings in Section 6.

2. The EMUS Instrument

The orbit of the EMM Hope probe has an apoapsis at 42,650 km and periapsis at 19,970 km with a 54.5 hr period. This high altitude orbit affords a synoptic view of Mars with full local time coverage every 9–10 days (Holsclaw et al., 2021). High and low resolution slits have angular widths of 0.18° and 0.25° and spectral widths of 1.3 and 1.8 nm, respectively (Holsclaw et al., 2021). EMUS remotely senses the thermosphere observing far-ultraviolet (FUV) emissions (see Figures 1 and 2) from hydrogen (H I 121.6 nm—Lyman α), oxygen (O I 130.4 and 135.6 nm), and (CO 4PG 140–170 nm). For the present analysis, we utilize EMUS U-OS1 and U-OS2 disk observations covering 20 February 2021 to 20 February 2022.

3. FUV Spectroscopy

We provide a brief overview of the calculation of emission feature intensities from observed EMUS spectra that are used as input to the $\Sigma CO/CO_2$ algorithm described below. The various emission sources present in the FUV
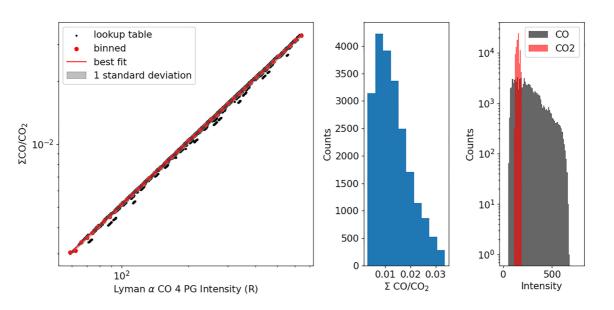
Figure 1. Left: Ratio of modeled carbon monoxide (CO) Fourth Positive Group column emission rates (Rayleighs) produced by CO as a function of $\Sigma CO/CO_2$ column density ratio. Model values are shown as black dots and correspond to an SZA of 0° and EMA of 0°. The scatter seen in the model ratios is due to variations in N_2 and Ar mixing ratios. Center: Histogram of lookup table $\Sigma CO/CO_2$ column density ratios. Right: Histogram of CO (gray) and CO_2 (red) lookup table intensities (Rayleighs) for SZA and EMA <35°.

spectrum are unblended using a multiple linear regression (MLR) process. This process is similar to that used for the Imaging Ultraviolet Spectrograph (IUVS; McClintock et al., 2015) onboard MAVEN (Jain et al., 2015; Stevens et al., 2015) with adjustments for the characteristics of the EMUS instrument. The AURIC model is used to generate synthetic spectra (hereafter templates) that represent the relative shape expected for each emission process. These templates are used as input to an MLR process tailored for Poisson statistics to distinguish the contribution of each of the known excitation processes. Intensities for specific sources of the CO 4PG band system are retrieved as part of the MLR process (see Figure S1 in Supporting Information S1).

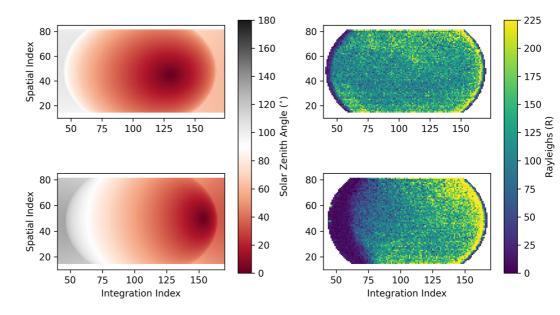

Figure 2. Solar zenith angles (left) and solar Lyman α excited carbon monoxide Fourth Positive Group intensity (right) for the second swath (out of three) for OS-2 observations on 24 April 2021 (top row) and 18 June 2021 (bottom row).

4. $\Sigma CO/CO_2$

4.1. Algorithm

The spectrum of CO 4PG includes emission arising from several physical processes: electron impact on CO and CO_2, electron impact dissociation and photodissociation of CO_2, as well as electron impact excitation and photoexcitation of CO by strong emission lines in the solar spectrum (Fox & Dalgarno, 1979). When considered individually, each of these processes result in CO 4PG emission spectra that have distinct shapes, that is, the bands of the 4PG system are excited differently for each process. Separating the intensities of each source allows for the identification of strong spectral features that can be used as diagnostics for the abundance of CO or CO_2 in the atmosphere. For example, direct excitation by solar emission lines producing 4PG emission only arises from allowed transitions in ground state CO molecules and can therefore be used as a direct measure of the abundance of CO in the Martian atmosphere.

Use of the CO 4PG band system to directly infer CO abundance in planetary atmospheres was first proposed by Kassal (1975, 1976). An important source of photoexcitation identified by Kassal is the strong solar Lyman α emission line that is scattering by the CO 4PG (14, 0) band and constitutes a significant portion of the total absorption at high CO column densities. The first detailed investigation of CO 4PG emission from planetary atmospheres was by Durrance (1981) using Venus dayglow observations by Pioneer Venus as well as the International Ultraviolet Explorer. The CO 4PG band system has also been utilized for analysis of comet observations (Feldman et al., 2018; Lupu et al., 2007). Here we make the first attempt to infer CO relative abundance using dayglow observations of CO 4PG emission at Mars.

Following the suggestion of Kassal and the detailed analysis by Durrance at Venus, we take advantage of CO 4PG excited by solar Lyman α (hereafter referred to as $I_{4PG(Ly\alpha)}$) to infer $\Sigma CO/CO_2$. The bottom panel of Figure S1 in Supporting Information S1 shows the CO 4PG spectrum resulting from fluorescent scattering of solar Lyman α photons by the CO 4PG (14,0) band. We specifically focus on the bright (14, 4) band at 135.2 nm. This band blends with emission from the O I 135.6 nm doublet and the N_2 LBH (3,0) band at 135.4 nm (see unblended EMUS spectrum in the top panel of Figure S1 in Supporting Information S1). Feldman et al. (2000) concluded that most of the blended emission is due to CO. AURIC model calculations using column densities of 10^{17} and 10^{19} cm^{-2} ($\sim$80 km) for CO and CO_2, respectively, support this conclusion.

Figure 1 shows the relationship between $I_{4PG(Ly\alpha)}$ and $\Sigma CO/CO_2$. While the relationship appears nearly linear, its exact functional form is not critical for the present discussion and will be addressed further in Section 4.2. It is sufficient to note that the relationship is single valued, that is, a given $I_{4PG(Ly\alpha)}$ maps to a single value of $\Sigma CO/CO_2$ (with a small uncertainty given by the scatter of points). This allows for the unambiguous determination of the relative composition of the atmosphere from an observed $I_{4PG(Ly\alpha)}$.

Forward modeling can be used to determine the relationship between $I_{4PG(Ly\alpha)}$ and $\Sigma CO/CO_2$, which can be stored in precomputed lookup tables to allow for fast computation. The forward modeling assumes an arbitrary reference solar Lyman α flux, $F_{Ly\alpha}^{ref}$, that is unlikely to precisely match the actual solar Lyman α flux, $F_{Ly\alpha}^{obs}$, at the time of any particular EMUS observation. Since $I_{4PG(Ly\alpha)}$ varies with both the solar Lyman α flux and the abundance of atmospheric CO, the former must be accounted for explicitly so that changes in $I_{4PG(Ly\alpha)}$ can be unambiguously attributed to the changes in the CO abundance. Representing the relationship in abstract form, we can write

$$\sum \frac{CO}{CO_2} = f\left(\frac{F_{Ly\,\alpha}^{obs}}{F_{Ly\,\alpha}^{ref}} I_{4PG(Ly\alpha)}^{ref}, \theta, \epsilon \right) \qquad (1)$$

where θ and ϵ are the solar zenith angle and emission angle, respectively, and the first term is the modeled intensity (corresponding to $F_{Ly\alpha}^{ref}$) scaled by the ratio of the observed to the reference solar Lyman α flux.

It is important to note the significance of the reference depth. There is no single correct reference depth to use when calculating a column density ratio. However, the reference depth should be large enough to encompass the region of the atmosphere where most of the emission originates from, while at the same time minimizing the uncertainty in the derived column density ratio. The main effect of selecting a different reference depth is to change the estimated uncertainty in the derived column density ratio. Clearly the absolute value of the derived column density ratio will change when using a difference reference depth, however this will have little impact on the main utility of a column density ratio. The column density ratio is most useful as a measure of relative change

in the state of the atmosphere, and the absolute value of a column density ratio has little inherent meaning except in relation to other measures of column density ratios.

Another important consideration that must be kept in mind is that knowledge of the column density ratio alone does not give any insight into the composition of the atmosphere at a particular altitude above the Martian surface. The algorithm is essentially one dimensional and does not measure the depth in terms of units of length (e.g., kilometers), therefore it is more useful to think in terms of column density or pressure. Based on AURIC model simulations, we determined that a CO_2 column depth of 5×10^{19} cm^{-2} is sufficiently deep enough to encompass the region of the atmosphere where most of the $I_{4PG(Ly\alpha)}$ emission originates from (see Figure S2 in Supporting Information S1). While this reference column depth is fixed in pressure space ($\sim$8.5 mPa), the corresponding altitude varies on the order of $\sim$15 km, with a mean value of $\sim$70 km.

4.2. Lookup Tables

Precomputed lookup tables are used to convert CO intensity, retrieved from the EMUS MLR process, to $\Sigma CO/CO_2$. A one dimensional photochemical model of the Martian atmosphere (see Supporting Information S1) is used to generate model atmospheres that serve as input to the forward model calculations that comprise the lookup table. Inputs to the photochemical model are varied to cover the range of expected values. The input parameters, the range of values used, and step size are:

- N_2 mixing ratio in the lower atmosphere: 0.02 to 0.04, 0.004 step.
- Mesospheric temperature: 150–350 K, step size 20 K.
- Exobase temperature: 150 K, 175 K, and 200 K.
- CO_2 photodissociation frequency at the top of the atmosphere: scale nominal rate of 3×10^7 s^{-1} by scale factors 0.2 to 5.0, step size of 0.4.
- Eddy diffusion coefficient: 17 values between 10^{13} and 10^{14} cm^2 s^{-1}.

Atmospheres generated by the photochemical model are constrained using CO_2, N_2 and O number densities and number density ratios at 140 km from IUVS periapse limb scan retrievals (Evans et al., 2015; Stevens et al., 2015). Model atmospheres with values outside the range seen in IUVS data are excluded from further consideration. The constraints applied are:

- $1.1 \times 10^9 < [CO_2] < 1.5 \times 10^{11}$ cm^{-3}.
- $9.5 \times 10^7 < [N_2] < 4 \times 10^9$ cm^{-3}.
- $3.5 \times 10^7 < [O] < 3.8 \times 10^9$ cm^{-3}.
- $0.01 < [N_2]/[CO_2] < 0.14$.
- $0.007 < [O]/[CO_2] < 0.07$.

where all number densities are at 140 km. The application of these constraints excludes about 20% of the parameter space. The remaining $\sim$20,000 atm are then used as input to AURIC to create synthetic spectra over a range of solar zenith and emission angles for each set of input parameters.

The lookup table containing modeled intensities and column density ratios (along with other ancillary information) is used in the data processing pipeline to convert intensities observed by EMUS into $\Sigma CO/CO_2$. Each point in the solar zenith and emission angle grid is a collection of {intensity, $\Sigma CO/CO_2$} values. In order to use these values with observed intensities, a functional dependence between $\Sigma CO/CO_2$ and intensity must be determined. Using bins logarithmically spaced in CO intensity, the mean modeled $\Sigma CO/CO_2$ is calculated for each bin (red circles in Figure 1). Then a curve is fit to the binned {intensity, $\Sigma CO/CO_2$} values using a least squares fit with Levenberg-Marquardt optimization. Linear, power law, and exponential functions were tested, and while all three functional forms generally represent the relationship well, an exponential of the form $ae^{-bx} + c$ fits the region of low intensity (low $\Sigma CO/CO_2$) best. As can be seen in Figure 1, for a given intensity, there is a range of possible values for $\Sigma CO/CO_2$. This spread is due to the range of input parameters used with the photochemical model, with the N_2 mixing ratio parameter being primarily responsible for the variation within a given CO intensity bin. The standard deviation of $\Sigma CO/CO_2$ in each bin is calculated and another exponential function is fit to those binned values. The gray shaded region in Figure 1 represents one standard deviation around the binned mean values.
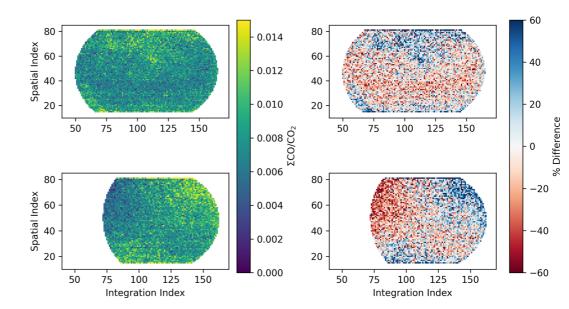
Figure 3. Retrieved $\Sigma CO/CO_2$ (left) and percent difference from swath averaged $\Sigma CO/CO_2$ (right) for the observations shown in Figure 2.

4.3. Level 3 CO/CO2 Data

EMUS Level 3 data files contain $\Sigma CO/CO_2$ derived from EMUS observations. The algorithm is primarily intended for the U-OS1 observations, though it may be applied to U-OS2 observations as well, or any EMUS observation that views the disk of Mars. We note that the spatial resolution for other EMUS observation types is typically too coarse to derive useful data products. U-OS1 is comprised of two scans, each scan imaging a little more than half the Martian disk visible from EMUS' vantage point. U-OS2 observations consist of three scans, with one scan covering approximately two thirds of the Martian disk, while the first and last scans cover the edges of the disk. $\Sigma CO/CO_2$ and viewing geometry (e.g., SZA, emission angle, etc.) are contained in the Level 3 FITS files. Before ingestion by the $\Sigma CO/CO_2$ algorithm, Level 2 data may be spatially binned to increase signal to noise. The algorithm is not applied to pixels with emission angles greater than 75° or solar zenith angles greater than 80° where an assumption of isotropic solar illumination becomes invalid. It is also important to note that a calibration error was identified by the EMUS team after the release of Level 2B data. A scale factor of 1.25 has been applied to the CO 4PG intensities used in this study to account for this error.

Figure 2 shows the solar zenith angle and the intensity of CO 4PG excited by solar Lyman α on the left and right, respectively. The upper row shows values for the central swath of an OS-2 observation from 24 April 2021, while the bottom row shows the central swath from an OS-2 observation on 18 June 2021. The left column of Figure 3 shows $\Sigma CO/CO_2$ derived from the algorithm described above, while the right hand column shows the percent difference of each pixel from the mean swath value. Variations in CO brightness with irregular shapes and corresponding relative abundance are observed in ∼25% of EMUS disk images. The patches of enhanced CO brightness display some local time and hemispheric asymmetry in their occurrence rates and are most likely due to changes in composition and photoelectron flux.

Random uncertainty values for $\Sigma CO/CO_2$ are based on the random uncertainties of the intensities input to the algorithm. The column density ratio random uncertainties are estimated using the range of column density ratio values derived by varying the input intensities $\pm$ one standard deviation of the intensity random uncertainties. Random uncertainties for the CO 4PG Lyman α intensities are ∼25%, which translates to random uncertainties for derived $\Sigma CO/CO_2$ of ∼50%. In addition to the random uncertainties there are systematic model uncertainties that must be considered. One source of model uncertainty arises from fitting the column density ratio versus intensity curves in the lookup table, described in Section 4.2. As seen in Figure 1 the lookup table curves do not exhibit much scatter and the model uncertainty here is ∼5%. There are also model uncertainties due to uncertainties in measured cross sections, which are estimated to be ±25% (Avakyan et al., 1999; Gronoff et al., 2012; Majeed & Strickland, 1997).
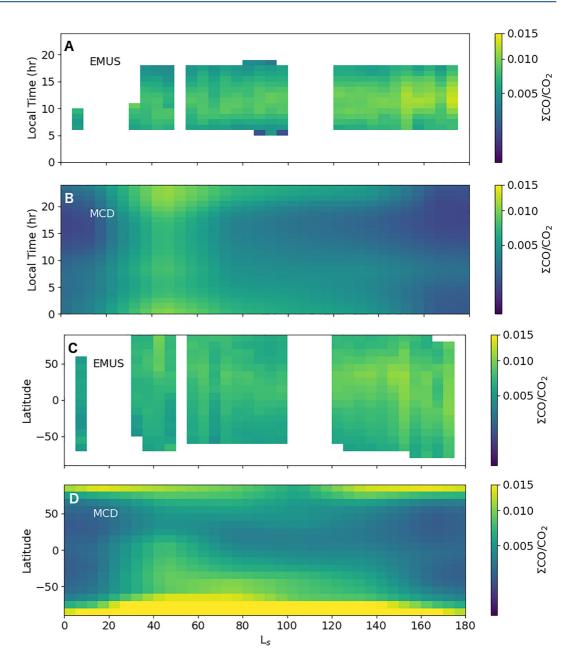
Figure 4. Comparison of mean Emirates Ultraviolet Spectrometer (EMUS) behavior and Mars Climate Database (MCD) model values as functions of L_s, latitude and local time. Panels A and B show mean EMUS and MCD values binned in local time and L_s, while Panels C and D show mean EMUS and MCD values binned in latitude and L_s.

5. Validation

The Mars Climate Database (MCD; Forget et al., 1999; González-Galindo et al., 2015; Millour et al., 2018) is a climatological database derived from the Laboratoire de Météorologie Dynamique du CNRS General Circulation Model (LMD-GCM). EMUS $\Sigma CO/CO_2$ values are compared with those derived from MCD version 5.3 as two dimensional maps in Figure 4. MCD column densities are calculated by generating density profiles using a solar minimum climatology. The top two panels show column density ratios as functions of L_s and local time of observation points, while the bottom two panels show column density ratios as functions of L_s and latitude (longitude and local time are held fixed because MCD variability with respect to these variables is relatively weak). For the L_s-local time images, the average values of EMUS data grouped into bins 5° of L_s and 1 hr local time are shown. For L_s-latitude images, mean values from 5° L_s to 10° of latitude bins are shown (between −90° and +90°

latitude). In both cases, MCD model values are calculated for all bins in the 2 dimensional grid, including those for which no EMUS data is available. For the L_s-latitude image, a fixed longitude of 0° and local time of 10:00 hr was used for input to the MCD model, while for the L_s-local time image the input longitude and latitude are set to 0°.

The mean absolute magnitude of EMUS $\Sigma CO/CO_2$ is systematically larger than MCD by ∼40%. This discrepancy is at least partially due to a CO surface abundance of 800 ppmv assumed by MCD. This value is now considered to be low by 30–40% based on recent observations by the Nadir Occultation for MArs Discovery instrument suite (NOMAD; Vandaele et al., 2015, 2018; Yoshida et al., 2022) on-board the ExoMars TGO, which suggest that the mean CO surface abundance is closer to 1,000–1,200 ppmv (Smith et al., 2021). Results from NOMAD are consistent with results from ACS MIR on ExoMars TGO (Olsen et al., 2021). The variability of observed relative CO abundance in local time and latitude for $0° < L_s < 180°$ is generally inconsistent with MCD 5.3 predictions. This may be due to a lack of dynamical constraints in MCD 5.3 that drive CO variability because of a lack of direct measurements of CO abundance in the thermosphere of Mars (100–160 km). Though we find these differences interesting, the cause of the discrepancy in behavior is beyond the scope of this paper and will be addressed in a future study using updated versions of MCD with dynamical constraints based on new information now available from ExoMars TGO, MAVEN, EMM, and other assets at Mars.

6. Summary

EMUS' vantage point from high orbit provides large scale, high cadence, synoptic views of Mars. In this paper we have presented an overview of the EMUS $\Sigma CO/CO_2$ data product. Though the basic algorithm has a rich heritage of terrestrial applications in the form of $\Sigma O/N_2$, some adjustments are required for application to the EMUS data set observed at Mars. We find that significant variability in CO brightness and relative column abundance is regularly observed in EMUS disk images. While the magnitude of EMUS $\Sigma CO/CO_2$ agrees with MCD 5.3 (corrected for a systematically low estimate of surface CO abundance), EMUS observed variability of CO relative column abundance in local time, latitude, and solar longitude is generally inconsistent with MCD predictions.

Notation

$\Sigma CO/CO_2$ The ratio of the vertical column density of CO above the altitude where the column density of carbon dioxide is equal to the reference depth. We adopt the notation $\Sigma CO/CO_2$ after Meier et al. (2005). This notation is preferred to simply CO/CO_2, which is ambiguous and may be confused with the volume density ratio at a specific altitude (which should be written as $[CO]/[CO_2]$).

Data Availability Statement

The EMUS Level 2A data used in this study are available at the Emirate Mars Mission Science Data Center (Amiri et al., 2022; Holsclaw et al., 2021) at https://sdc.emiratesmarsmission.ae/data/emus. Users of EMUS disk data are reminded to carefully read documentation and release notes for detailed information regarding DQI flag values, limitations of the data, etc. The MAVEN IUVS processed (Level 1C) and derived (Level 2) data are publicly available in FITS format on the NASA Planetary Data System (PDS) at https://doi.org/10.17189/1518964 (Schnieder, 2021b) and https://doi.org/10.17189/1518956 (Schnieder, 2021a), respectively. MAVEN EUVM Level 2 data are available at the LASP MAVEN Science Data Center server (Eparvier, 2022), https://lasp.colorado.edu/maven/sdc/public/pages/search/search.html. Derived column density ratios and corresponding uncertainties can be obtained from https://data-sdc-publications-mbrsc.s3.eu-west-1.amazonaws.com/emm_emu_l3disk_grl.tar.gz.

References

Almatroushi, H., AlMazmi, H., AlMheiri, N., AlShamsi, M., AlTunaiji, E., Badri, K., et al. (2021). Emirates Mars mission characterization of Mars atmosphere dynamics and processes. *Space Science Reviews*, *217*(8), 1–31. https://doi.org/10.1007/s11214-021-00851-6

Amiri, H., Brain, D., Sharaf, O., Withnell, P., McGrath, M., Alloghani, M., et al. (2022). The emirates Mars mission. *Space Science Reviews*, *218*(1), 1–46. https://doi.org/10.1007/s11214-021-00868-x

Avakyan, S., Ii'In, R. N., Lavrov, V. M., & Ogurtsov, G. N. (1999). *Collision processes and excitation of UV emission from planetary atmospheric gases: A handbook of cross sections*. CRC.

Barth, C., Fastie, W., Hord, C., Pearce, J., Kelly, K., Stewart, A., et al. (1969). Mariner 6: Ultraviolet spectrum of Mars upper atmosphere. *Science*, *165*(3897), 1004–1005. https://doi.org/10.1126/science.165.3897.1004

Correira, J., Evans, J. S., Lumpe, J. D., Krywonos, A., Daniell, R., Veibell, V., et al. (2021). Thermospheric composition and solar EUV flux from the global-scale observations of the limb and disk (GOLD) mission. *Journal of Geophysical Research*, *126*(12), e29517. https://doi.org/10.1029/2021JA029517

Durrance, S. T. (1981). The carbon monoxide fourth positive bands in the Venus dayglow. I—Synthetic spectra. *Journal of Geophysical Research*, *86*(A11), 9115–9124. https://doi.org/10.1029/JA086iA11p09115

Encrenaz, T., Fouchet, T., Melchiorri, R., Drossart, P., Gondet, B., Langevin, Y., et al. (2006). Seasonal variations of the Martian co over Hellas as observed by omega/Mars express. *Astronomy & Astrophysics*, *459*(1), 265–270. https://doi.org/10.1051/0004-6361:20065586

Eparvier, F. (2022). MAVEN EUV Modelled Data Bundle [Dataset]. NASA Planetary Data System. https://doi.org/10.17189/1517691

Evans, J. S., Stevens, J. D., Lumpe, M. H., Schneider, N. M., Stewart, A. I. F., Deighan, J. I., et al. (2015). Retrieval of CO_2 and N_2 in the Martian thermosphere using dayglow observations by IUVS on MAVEN. *Geophysical Research Letters*, *42*(21), 9040–9049. https://doi.org/10.1002/2015gl065489

Evans, J. S., Strickland, D. J., & Huffman, R. E. (1995). Satellite remote sensing of thermospheric O/N_2 and solar EUV. 2: Data analysis. *Journal of Geophysical Research*, *100*(A7), 12227. https://doi.org/10.1029/95JA00573

Feldman, P. D., Burgh, E. B., Durrance, S. T., & Davidsen, A. F. (2000). Far-ultraviolet spectroscopy of Venus and Mars at 4 Å resolution with the Hopkins ultraviolet telescope on Astro-2. *The Astrophysical Journal*, *538*(1), 395–400. https://doi.org/10.1086/309125

Feldman, P. D., Weaver, H. A., A'Hearn, M. F., Combi, M. R., & Russo, N. D. (2018). Far-ultraviolet spectroscopy of recent comets with the cosmic origins spectrograph on the Hubble Space Telescope. *The Astronomical Journal*, *155*(5), 193. https://doi.org/10.3847/1538-3881/aab78a

Forget, F., Hourdin, F., Fournier, R., Hourdin, C., Talagrand, O., Collins, M., et al. (1999). Improved general circulation models of the Martian atmosphere from the surface to above 80 km. *Journal of Geophysical Research*, *104*(E10), 24155–24176. https://doi.org/10.1029/1999JE001025

Fox, J. L., & Dalgarno, A. (1979). Ionization, luminosity, and heating of the upper atmosphere of Mars. *Journal of Geophysical Research*, *84*(A12), 7315–7333. https://doi.org/10.1029/JA084iA12p07315

González-Galindo, F., López-Valverde, M. A., Forget, F., García-Comas, M., Millour, E., & Montabone, L. (2015). Variability of the Martian thermosphere during eight Martian years as simulated by a ground-to-exosphere global circulation model. *Journal of Geophysical Research*, *120*(11), 2020–2035. https://doi.org/10.1002/2015JE004925

Gronoff, G., Simon Wedlund, C., Mertens, C. J., Barthélemy, M., Lillis, R. J., & Witasse, O. (2012). Computing uncertainties in ionosphere-airglow models: II. The Martian airglow. *Journal of Geophysical Research*, *117*(A5), 5309. https://doi.org/10.1029/2011JA017308

Holmes, J. A., Lewis, S. R., Patel, M. R., & Smith, M. D. (2019). Global analysis and forecasts of carbon monoxide on Mars. *Icarus*, *328*, 232–245. https://doi.org/10.1016/j.icarus.2019.03.016

Holsclaw, G. M., Deighan, J., Almatroushi, H., Chaffin, M., Correira, J., Evans, J. S., et al. (2021). The emirates Mars ultraviolet spectrometer (EMUS) for the EMM mission. *Space Science Reviews*, *217*(8), 1–49. https://doi.org/10.1007/s11214-021-00854-3

Jain, S. K., Stewart, A. I. F., Schneider, N. M., Deighan, J., Stiepen, A., Evans, J. S., et al. (2015). The structure and variability of Mars upper atmosphere as seen in MAVEN/IUVS dayglow observations. *Geophysical Research Letters*, *42*(21), 9023–9030. https://doi.org/10.1002/2015GL065419

Jakosky, B. M., Lin, R. P., Grebowsky, J. M., Luhmann, J. G., Mitchell, D., Beutelschies, G., et al. (2015). The Mars atmosphere and volatile evolution (MAVEN) mission. *Space Science Reviews*, *195*(1), 3–48. https://doi.org/10.1007/s11214-015-0139-x

Kaplan, L. D., Connes, J., & Connes, P. (1969). Carbon monoxide in the Martian atmosphere. *The Astrophysical Journal*, *157*, L187. https://doi.org/10.1086/180416

Kassal, T. T. (1975). Resonant fluorescent scattering of solar radiation by the fourth positive band system of CO. *Applied Optics*, *14*(7), 1513–1515. https://doi.org/10.1364/AO.14.001513

Kassal, T. T. (1976). Scattering of solar Lyman alpha by the/14.0/band of the fourth positive system of CO. *Journal of Geophysical Research*, *81*(7), 1411–1412. https://doi.org/10.1029/JA081i007p01411

Krasnopolsky, V. A. (2003). Spectroscopic mapping of Mars co mixing ratio: Detection of north-south asymmetry. *Journal of Geophysical Research*, *108*(E2). https://doi.org/10.1029/2002je001926

Krasnopolsky, V. A. (2007). Long-term spectroscopic observations of Mars using IRTF/CSHELL: Mapping of O_2 dayglow, CO, and search for CH_4. *Icarus*, *190*(1), 93–102. https://doi.org/10.1016/j.icarus.2007.02.014

Leblanc, F., Witasse, O., Winningham, J., Brain, D., Lilensten, J., Blelly, P.-L., et al. (2006). Origins of the Martian aurora observed by spectroscopy for investigation of characteristics of the atmosphere of Mars (SPICAM) on board Mars express. *Journal of Geophysical Research*, *111*(A10), 9313. https://doi.org/10.1029/2006JA011763

Lefèvre, F., & Krasnopolsky, V. (2017). Atmospheric photochemistry. *The atmosphere and climate of Mars*, *18*, 405–432. https://doi.org/10.1017/9781139060172.013

Lupu, R. E., Feldman, P. D., Weaver, H. A., & Tozzi, G.-P. (2007). The fourth positive system of carbon monoxide in the Hubble Space Telescope spectra of comets. *The Astrophysical Journal*, *670*(2), 1473–1484. https://doi.org/10.1086/522328

Mahaffy, P. R., Benna, M., Elrod, M., Yelle, R. V., Bougher, S. W., Stone, S. W., & Jakosky, B. M. (2015). Structure and composition of the neutral upper atmosphere of Mars from the MAVEN NGIMS investigation. *Geophysical Research Letters*, *42*(21), 8951–8957. https://doi.org/10.1002/2015gl065329

Majeed, T., & Strickland, D. J. (1997). New survey of electron impact cross sections for photoelectron and auroral electron energy loss calculations. *Journal of Physical and Chemical Reference Data*, *26*(2), 335–349. https://doi.org/10.1063/1.556008

McClintock, W. E., Schneider, N. M., Holsclaw, G. M., Clarke, J. T., Hoskins, A. C., Stewart, I., et al. (2015). The imaging ultraviolet spectrograph (IUVS) for the MAVEN mission. *Space Science Reviews*, *195*(1–4), 75–124. https://doi.org/10.1007/s11214-014-0098-7

Meier, R. R., Crowley, G., Strickland, D. J., Christensen, A. B., Paxton, L. J., Morrison, D., & Hackert, C. L. (2005). First look at the 20 November 2003 superstorm with TIMED/GUVI: Comparisons with a thermospheric global circulation model. *Journal of Geophysical Research*, *110*(A9), 9. https://doi.org/10.1029/2004JA010990

Millour, E., Forget, F., Spiga, A., Vals, M., Zakharov, V., Montabone, L., et al. (2018). The Mars climate database (version 5.3). In *From mars express to exomars*. 68.

Olsen, K., Lefèvre, F., Montmessin, F., Fedorova, A., Trokhimovskiy, A., Baggio, L., et al. (2021). The vertical structure of CO in the Martian atmosphere from the Exomars Trace Gas Orbiter. *Nature Geoscience*, *14*(2), 67–71. https://doi.org/10.1038/s41561-020-00678-w

Schnieder, N. (2021). MAVEN IUVS processed-level data product bundle [Dataset]. NASA Planetary Data System. https://doi.org/10.17189/1518964

Smith, M. D., Daerden, F., Neary, L., & Khayat, A. (2018). The climatology of carbon monoxide and water vapor on Mars as observed by CRISM and modeled by the GEM-Mars general circulation model. *Icarus*, *301*, 117–131. https://doi.org/10.1016/j.icarus.2017.09.027

Smith, M. D., Daerden, F., Neary, L., Khayat, A. S., Holmes, J. A., Patel, M. R., et al. (2021). The climatology of carbon monoxide on Mars as observed by NOMAD nadir-geometry observations. *Icarus*, *362*, 114404. https://doi.org/10.1016/j.icarus.2021.114404

Smith, M. D., Wolff, M. J., Clancy, R. T., & Murchie, S. L. (2009). Compact reconnaissance imaging spectrometer observations of water vapor and carbon monoxide. *Journal of Geophysical Research*, *114*(E2), E00D03. https://doi.org/10.1029/2008je003288

Sprague, A. L., Boynton, W., Kerry, K., Janes, D., Hunten, D., Kim, K., et al. (2004). Mars' south polar Ar enhancement: A tracer for south polar seasonal meridional mixing. *Science*, *306*(5700), 1364–1367. https://doi.org/10.1126/science.1098496

Sprague, A. L., Boynton, W. V., Forget, F., Lian, Y., Richardson, M., Starr, R., et al. (2012). Interannual similarity and variation in seasonal circulation of Mars' atmospheric Ar as seen by the Gamma Ray Spectrometer on Mars Odyssey. *Journal of Geophysical Research*, *117*(E4). https://doi.org/10.1029/2011je003873

Stevens, M. H., Evans, J. S., Lumpe, J., Westlake, J. H., Ajello, J. M., Bradley, E. T., & Esposito, L. W. (2015). Molecular nitrogen and methane density retrievals from Cassini UVIS dayglow observations of Titan's upper atmosphere. *Icarus*, *247*, 301–312. https://doi.org/10.1016/j.icarus.2014.10.008

Strickland, D. J., Bishop, J., Evans, J. S., Majeed, T., Shen, P. M., Cox, R. J., et al. (1999). Atmospheric ultraviolet radiance integrated code (AURIC): Theory, software architecture, inputs, and selected results. *Journal of Quantitative Spectroscopy and Radiative Transfer*, *62*(6), 689–742. https://doi.org/10.1016/S0022-4073(98)00098-3

Strickland, D. J., Evans, J. S., & Paxton, L. J. (1995). Satellite remote sensing of thermospheric O/N_2 and solar EUV. 1: Theory. *Journal of Geophysical Research*, *100*(A7), 12217. https://doi.org/10.1029/95JA00574

Vandaele, A. C., Lopez-Moreno, J.-J., Patel, M. R., Bellucci, G., Daerden, F., Ristic, B., et al. (2018). NOMAD, an integrated suite of three spectrometers for the Exomars trace gas mission: Technical description, science objectives and expected performance. *Space Science Reviews*, *214*(5), 1–47. https://doi.org/10.1007/s11214-018-0517-2

Vandaele, A. C., Neefs, E., Drummond, R., Thomas, I. R., Daerden, F., Lopez-Moreno, J.-J., et al. (2015). Science objectives and performances of nomad, a spectrometer suite for the Exomars TGO mission. *Planetary and Space Science*, *119*, 233–249. https://doi.org/10.1016/j.pss.2015.10.003

Yoshida, N., Nakagawa, H., Aoki, S., Erwin, J., Vandaele, A. C., Daerden, F., et al. (2022). Variations in vertical CO/CO_2 profiles in the Martian mesosphere and lower thermosphere measured by the Exomars TGO/NOMAD: Implications of variations in eddy diffusion coefficient. *Geophysical Research Letters*, *49*(10), e2022GL098485. https://doi.org/10.1029/2022gl098485